Determination of the Pitching Characteristics of Tumbling Bodies by the Free-Rotation Method

Takashi Yoshinaga,* Kenji Inoue,† and Atsushi Tate‡
National Aerospace Laboratory, Tokyo, Japan

A method to determine the pitching moment of slender bodies with less support interference was developed by simulating a pitching motion of 1-DOF angular motion in wind tunnels. The pitching moment acting on the bodies was determined to be a one-valued function of the angle of attack α and its time derivative α'. A phase plane concept proved to be useful in the analysis of the pitching motion. It was possible to calculate the pitching motion for an arbitrary initial condition by using the mathematical expression of the moment. The variation of energy in the pitching motion showed the energy exchange between the models and the air flow. The visualization of the wake flowfield revealed the hysteresis of the separated flow about the model which caused the amplification of the pitching motion. The effects of the shapes of models, freestream velocity, and the center of gravity on the pitching moment coefficients were investigated.

Nomenclature

$A_m(\alpha)$ = coefficients of polynomials
a_{mn}, b_m = coefficients of Fourier series
c.g. = center of gravity
C_m = pitching moment coefficient, m/qSl
D = diameter
$E(t)$ = total energy of pitching motion
E_0 = reference energy defined by an initial condition
I = moment of inertia of a body
l = model length
m = pitching moment
m_A = pitching moment due to aerodynamic force
m_F = impeding moment due to friction
q = dynamic pressure, $\rho V_\infty{}^2/2$
r_n = nose tip radius
S = reference area, $\pi D^2/4$
t = time
$U(\alpha)$ = potential energy of pitching motion
V_∞ = freestream velocity
$x_{c.g.}$ = distance from the tip to the center of gravity of a model
α = angle of attack
ρ = density
$\theta 1/2$ = nose half-angle
$()'$ = derivative with respect to time

Introduction

OVER the past ten years, studies of aerodynamic characteristics of slender bodies at high angles of attack have been conducted to ensure stable flight of vehicles and missiles.[1,2] Most of the studies have been carried out under static conditions and have proved to be useful in controlling the attitude of bodies at high angles of attack. However, to estimate the free angular and translational motions of falling bodies such as rocket heads without active control, one should use dynamically measured aerodynamic characteristics.[3]

To investigate the stability of recovering rocket heads, more than ten rocket head models were dropped from a helicopter at an altitude of 3.5 km.[4,5] Although it was expected that the models ($x_{c.g.} \cong 50\%$) would fall in a stable attitude parallel to the sea surface, different types of motion were observed. Just after the models were released, they showed pitching or tumbling motions with the axis parallel to the sea surface. Then most of them showed another type of rotation, a so-called flat spin, with the axis normal to the sea surface. Some calculations[6] were made and dynamic experiments conducted on flat spins[7] and coning motions.[8]

Complexity comes into the investigations of the pitching and tumbling motions as the angular motion exceeds the range of linear small-amplitude oscillation with respect to α and α'. Several measurements of the aerodynamic forces involved in the pitching motion of axisymmetric bodies have been made, including bodies at high angles of attack showing great amplitudes of oscillation. In Ref. 9, the unsteady motion was estimated by using the measured static aerodynamic coefficients and the average values of measurements taken while the body was rotating. In Ref. 10, it is clarified that when a slender body varies the angle of attack, the moment acting on it depends not only on angle of attack α but also on angular velocity α'. In Ref. 11, the autorotations of plates, cylindrical bodies, and other shapes were observed both in high- and low-speed flows. In Ref. 12, the pitching motion of fuel stores dropped from an airplane was analyzed. As a motion relevant to the tumbling motion of slender bodies, the well-known autorotation of wings and plates was experimentally investigated and the moments, lift forces, and drag forces were measured.[11,13,14] In the above-mentioned papers the analytical expressions of the pitching moment, which were obtained from the variation of time-dependent angles of attack or by the direct measurements of the moment in motion, seem too simple to reproduce the real angular motions.

The present paper describes a method of determining the unsteady pitching characteristics of bodies by conducting wind tunnel tests of 1-DOF free rotation of models. The concept of a phase plane is utilized successfully to express the pitching moment m by a one-valued function of the angle of attack α and angular velocity α'. This mathematical expression of m makes it possible to predict and investigate the characteristics of the angular motion of the body.

Submitted Dec. 17, 1982; revision received May 5, 1983.

*Head, Aerothermodynamics Section, First Aerodynamics Division. Member AIAA.
†Head, Boundary Layer Research Section, First Aerodynamics Division. Member AIAA.
‡Research Official, Aerothermodynamics Section, First Aerodynamics Division.

Procedure of Experiments

Study of the dynamics of a free-flight body shows that the motion of a body may be considered to be the sum of the translational motion of the center of gravity (c.g.) and the angular motion about the center. The fluctuating translational motion of a body of great mass, which is caused by the angular motion, is superposed on an averaged translational motion. If the fluctuation is assumed to be small compared with the averaged velocity, the angular motion of a body can be simulated in a wind tunnel by supporting a model of the body at its center of gravity, allowing it to rotate freely around this point.

It is observed that for a rocket-like body with the c.g. near its middle, the pitching motion exceeds the yawing motion around an equilibrium angle of attack near 90 deg in low-speed flow.[8] The investigation in this paper is limited to the pitching motion around an axis normal to a freestream and passing through the center of gravity. The model is allowed to rotate freely around the axis. In this case, the equation of the angular motion is generally expressed as

$$I\alpha'' = m = m_A(\text{shape}, \rho, V_\infty, \alpha, \alpha', \alpha'', \alpha''', \ldots) - m_F \quad (1)$$

When the impeding moment caused by the friction of the shaft m_F is negligibly small compared with m_A, m_A may be considered as the total moment acting on the body. The motion of the model and the protractor fixed on the opposite window were recorded on 16 mm film at a speed of 48 (for small models) or 32 (for a large model) frames/s.

Models and Experimental Facilities

Figure 1a shows models, made of acrylic resin, which were used for the pitching experiments in a small wind tunnel. The diameters of cone-cylinder models and bicone cylinder models are 25 mm, 135 mm long, tip radius 3 mm, and the half-nose angles 10, 15, and 20 deg. The cylinder models have a length of 120 mm and various diameters. To support the cone-cylinder models, holes of 1 mm diameter were drilled at points from 50 to 62.5% from the tip at intervals of 2.5% and the center of gravity was set to the point by moving the weights inside the model. The bicone cylinder, cylinder, and hemisphere-cylinder models were supported at the 50% point.

Figure 1b shows a larger cone-cylinder model of 50 mm diameter and 275 mm long. The base and nose sections, which have half-nose angles of 15 deg and blunted tips of 6 mm radius, are made of resin to reduce the weight of the model. The fuselage is made of a duralumin pipe 2 mm thick. Its support position was varied at intervals of about 2.5% over a range of 50-62.7% from the nose. Miniature ball bearings at the support position of the models reduced friction.

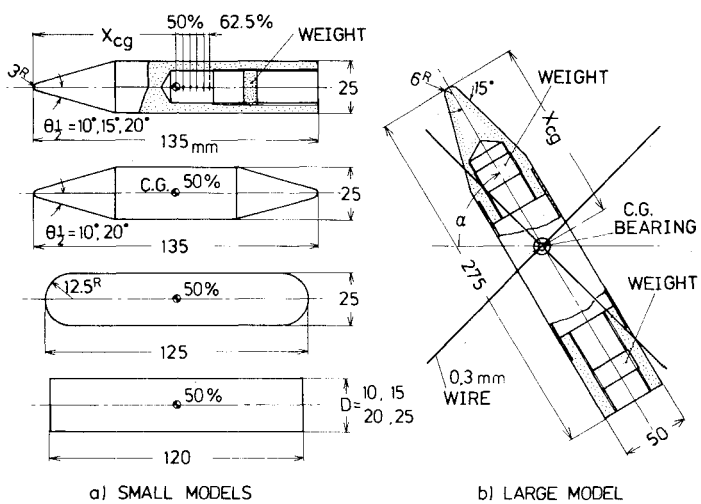

Fig. 1 Axisymmetric models supported at the center of gravity.

Models of 25 mm diameter were supported in a small wind tunnel that had a test cross section of 150×200 mm. In order to reduce interference of the supporting components on the flowfield and consequently on the pitching motion, the models were supported by a single steel wire 0.9 mm in diameter tightened across the test section perpendicular to the freestream. Since the wire passed through a small hole on the model normal to the body axis, the friction between the model and the wire was small and the model was able to rotate freely on the wire. The freestream velocity was adjustable up to 25 m/s. Although the interference between the wire and the models seemed to be small, the variation of the blockage ratio of the model during one rotation was rather large, ranging from 1.6 to 8%, which might have had some effect on the angular velocity. When a large model with a diameter of 50 mm was installed in a low-turbulence closed-return wind tunnel with a cross section of 550×650 mm, the variation of blockage ratio was reduced to a range of 0.55-2.7% in one rotation. The shaft of the model was supported by four steel wires on each side (eight wires in all).

Processing of Time-Dependent Angular Data

In this section, data for a standard cone-cylinder model ($l=135$ mm, $D=25$ mm, $\theta\frac{1}{2}=15$ deg, and $r_n=3$ mm) supported at a center of gravity of 55% is used to show how pitching motion data is processed. The angles of attack were read from each frame of movie film at every 0.5 deg. Figure 2a shows the time-dependent variation of the angle of attack starting from 268 deg at the freestream velocity of 10.5 m/s. When the installed model was released gently at equilibrium angles of attack near 90 and 270 deg, the model began pitching oscillations which increased in amplitude. After several pitching oscillations about the statically stable angle of attack, the model did an angular oscillation of greater amplitude about the angle of 0 deg. Following one cycle of the latter the model began to rotate and approached a steady rotation, i.e., repetition of the variation of the angle of attack between 0 and 360 deg in the same pattern. By differentiating the pitching angle numerically with respect to time, the pitching angular velocity $\alpha'(t)$ and the pitching angular acceleration $\alpha''(t)$ were obtained as functions of time. The results of differentiating α with respect to time, using a finite difference formula, will include a roundoff error due to the least unit of the read angle, and an error due to the finite difference formula. These errors should be minimized by choosing a

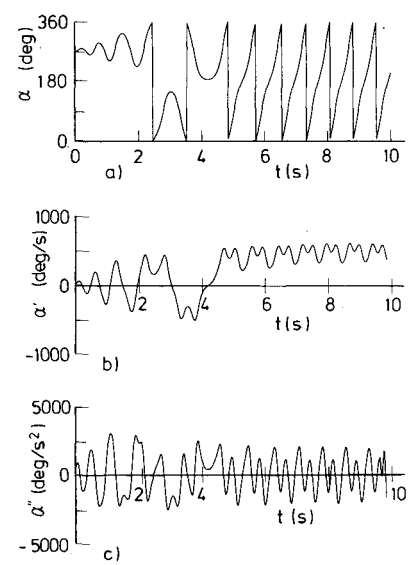

Fig. 2 Time-dependent angular motion of the standard cone-cylinder model about 55% c.g. ($\theta\frac{1}{2}=15$ deg, $D=25$ mm, $l=135$ mm, $I=586$ g.cm^2) at $V_\infty=10.5$ m/s. a) Angle of attack $\alpha(t)$. b) Angular velocity $\alpha'(t)$. c) Angular acceleration $\alpha''(t)$.

suitable interval of time and the proper finite difference formula. Numerical tests for analytical expressions similar to the variation of the pitching angle showed that a difference formula of order O (h^4) and an interval of 4-6 h will give good results, where h is the time interval between each frame of moving picture film. The differentiated values for each point were smoothed by the least-squares method, using the values in the front and rear. Figures 2b and 2c show the results obtained for the variation of angular velocity α' and the angular acceleration α'' by numerical differentiation. Figure 2c also shows that, even when the angular motion approaches a steady rotation, the moment takes positive and negative values so there is energy transfer between the model and the flow in a rotation.

Expression of the Pitching Motion on a Phase Plane

In general, the moment m_A depends on the angle of attack α and its derivatives α', α'', α''',..., but, in the present case, it is assumed to be a function of α and α' for a fixed value of the moment of inertia of the model at the freestream velocity. This assumption is justified later by experimental data. The expression of α'' on a phase plane (α, α') helps to understand the characteristics of the angular motion by taking time t as a parameter. In Fig. 3, two angular motions are drawn as trajectories on the phase plane (α, α'). The angular oscillation diverging about the equilibrium angle is expressed as a whirlpool on the phase plane, and the following greater oscillation around the angle of 0 deg is expressed as another whirlpool which includes the angle. As the model changed to a positive (clockwise) rotation, the trajectories on the plane became curves passing repeatedly from left to right in the upper section of the plane ($\alpha' > 0$), approaching a limiting curve for a steady rotation. For the counterclockwise rotation, the trajectory runs from right to left in the lower section ($\alpha' < 0$). The final direction of rotation cannot be predicted since it depends on the starting angles. This final trajectory of the rotation is classified as a limit cycle of the second kind. The points (0, 0) and (180 deg, 0) are considered saddle points. Even when other trajectories for different initial angles of attack under the same aerodynamic conditions are added to Fig. 3, none of the trajectories cross each other. This means that the angular motion or angular moment is defined by α and α' for a fixed value of the moment of inertia of the model. At each point on the trajectories, the angular acceleration α'' or moment of force m ($=I\alpha''$) governing the motion is defined. If we could carry out enough experiments to cover the phase plane with these trajectories, the curved surface of the moment on a phase plane (α, α') would be defined. In practice, it may be obtained by a suitable interpolation between the trajectories.

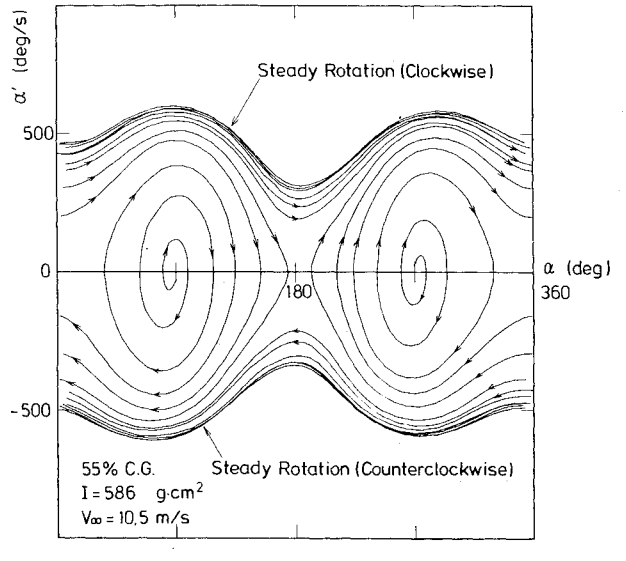

Fig. 3 Trajectories on a phase plane of two angular motions of the standard cone-cylinder model.

Moment Governing the Pitching Motion

To find the variation of the pitching moment at a constant angular velocity, pitching moment coefficients at the cross sections of the trajectories and the lines of constant α' in Fig. 3 were interpolated. Figure 4a shows the variation of pitching moment coefficient with α at $\alpha' = 0$ for which four trajectories were used. The values of $-C_m$ at the symmetric point with respect to (180 deg, 0) in the range $180 < \alpha < 360$ deg, are also plotted by solid circles. The amount of data is insufficient to cover all angles of attack, but additional tests with different initial conditions improve this situation. This figure also shows pitching moment coefficients measured statically by a six-component force balance for a similar cone-cylinder model ($l/D = 6$, $D = 65$ mm, $\theta/2 = 15$ deg) at Mach number 0.5 around the 55% c.g. point from the nose tip.[5]

Figure 4b shows the variation of the pitching moment coefficient with α for different α' where a suitable curve fit is used. Near the static equilibrium angle where α is approximately 90 deg, each curve shifts to the right as α' increases. This means that the attitude of the model is dynamically unstable, which is opposite to the results noted in Ref. 10. This may be attributed to the difference in the shape, especially to that in fineness ratio, Reynolds number, and the method of supporting the model.

Next, Fig. 5a shows the equimoment coefficient curves on the phase plane depicted by utilizing the experimentally obtained moment on the trajectory. The values of α'' at the intersections of lines of constant α at intervals of 2.5 deg and trajectories are obtained by interpolation. The values of α'' as a function of α' as a function of α' on each line of constant α

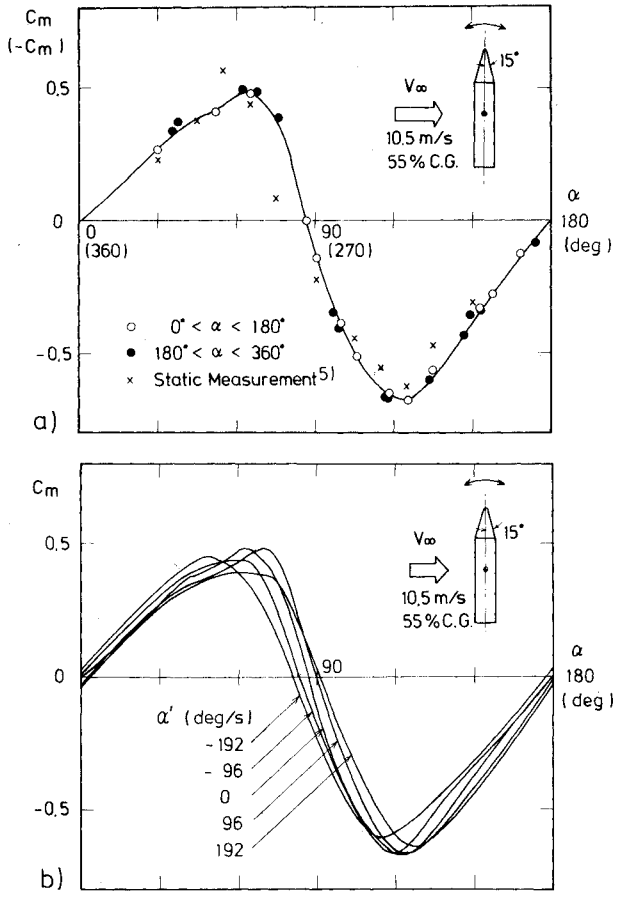

Fig. 4 Variation of pitching moment coefficient with angle of attack. a) $\alpha' = 0$. b) Different constant angular velocities.

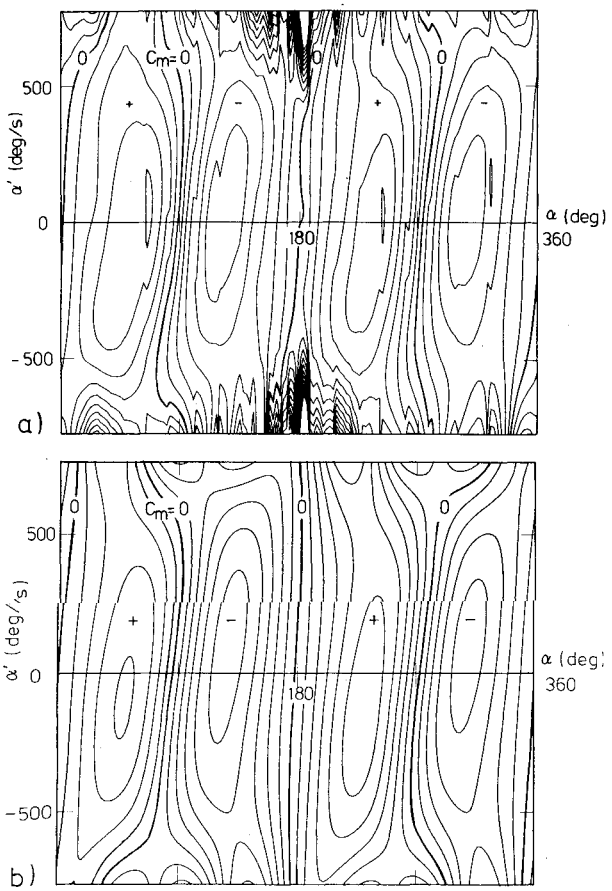

Fig. 5 Moment diagrams on a phase plane. The difference of C_m between lines equals 0.107. a) Experimentally obtained. b) Mathemetically represented.

are approximated by cubic or quartic polynomials by the method of least squares. Some pointed shapes of the equimoment curves do not reflect the real variation of the moment. The equimoment curves show that there are at least two maximum and two minimum points near $\alpha'=0$ in the range $0<\alpha<360$ deg, and that $|\alpha''|$ decreases as $|\alpha'|$ increases. The stability of the angular motion near the equilibrium points is summarized as follows. α_e is statically stable when $\partial m/\partial\alpha(\alpha_e, 0)<0$ and dynamically stable when $\partial m/\partial\alpha'(\alpha_e,0)<0$. It is statically unstable when $\partial m/\partial\alpha(\alpha_e,0)>0$ and dynamically unstable when $\partial m/\partial\alpha'(\alpha_e,0)>0$. Therefore, since the equimoment curves tilt to the right, the tested cone-cylinder model is found to be statically stable but dynamically unstable at equilibrium angles near $\alpha=90$ and 270 deg.

Mathematical Representation of the Pitching Moment

To analyze and discuss the nonlinear pitching motion of bodies by using data obtained from experiments, it is desirable that the right side of Eq. (1) be represented by a mathematical expression. On the phase plane (α, α') of Fig. 3, the abscissa in the range 0-360 deg is divided into equal intervals. The distributions of the angular acceleration α'' for several runs on each dividing line parallel to the ordinate indicate that α'' is a single-valued function of α and α' for a particular value of the moment of inertia of the model at the same aerodynamic condition. Polynomials of higher than the third order are necessary to approximate the data of α'' on the lines of constant α over the range $|\alpha'|\leq 600$ deg/s. The data are cruve fitted by polynomials using the least-squares method. Since the coefficients A_m of the resulting polynomials are periodical functions of α with the period of

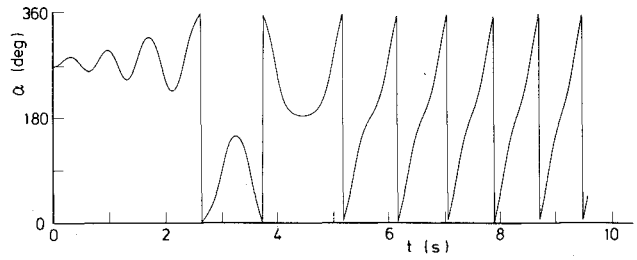

Fig. 6 Diverging angular motion of an angle of attack obtained by integrating the mathematical expression of moment of force.

360 deg, the coefficients A_m are expressed as Fourier series as follows:

$$\alpha''=A_0(\alpha)+A_1(\alpha)\alpha'+A_2(\alpha)\alpha'^2+\ldots+A_M(\alpha)\alpha'^M$$

$$=\sum_{m=0}^{M}\left[\frac{a_{m_0}}{2}+\sum_{n=1}^{N}(a_{mn}\cos n\alpha+b_{mn}\sin n\alpha)\right]\alpha'^m \qquad (2)$$

Multiplying both sides of Eq. (2) by $I\alpha'$, and integrating with respect to t, we obtain the following expression:

$$E(t)=I\frac{\alpha'^2}{2}+U(\alpha)=I\int_0^t\sum_{m=1}^{M}\left[\frac{a_m}{2}/\right.$$

$$\left.+\sum_{n=1}^{N}(a_{mn}\cos n\alpha+b_{mn}\sin n\alpha)\right]\alpha'^{m+1}dt+E_0 \qquad (3)$$

where

$$U(\alpha)=-I\left[\frac{a_{00}}{2}\alpha+\sum_{n=1}^{N}\frac{1}{n}\{a_{0n}\sin n\alpha+b_{0n}(1-\cos n\alpha)\}\right] \qquad (4)$$

The function $U(\alpha)$ is the sum of the terms independent of α' and is regarded as the potential energy of the pitching motion. The reference energy level is chosen so that $U(0)=0$. When α'' does not depend on α' the total energy E is conserved. The constant E_0 is determined by an initial condition. When $a_{00}\neq 0$, $U(\alpha)$ is not a single-valued function but it gains a constant value for every 360 deg period. The value of a_{00} is a measure of the tendency to rotate in one direction. This tendency may be caused by factors such as a small geometrical asymmetry of the model. Differentiating Eq. (3) with respect to t, we obtain

$$\frac{dE}{dt}=I\sum_{m=1}^{M}\left[\frac{a_{m0}}{2}+\sum_{n=1}^{N}(a_{mn}\cos n\alpha+b_{mn}\sin n\alpha)\right]\alpha'^{m+1} \qquad (5)$$

This gives the variation rate of the energy of the model. The whole domain of the phase plane is divided into regions according to the sign of E'. At the equilibrium point (α_e, 0), $dU/d\alpha=0$. Depending on whether $d^2U/d\alpha^2>0$ or <0, α_e is statically stable or unstable. Whether $E'<0$ or >0 also determines whether α_e is dynamically stable or unstable.

The above method is applied to the experimental data for a cone-cylinder model at a wind velocity of 10.5 m/s. In the calculation, data for four runs of angular motion, starting from rest and approaching steady rotation, were used. To get the value of a_{mn}, the range of α between 0 and 360 deg was divided into 36 segments and approximation by cubic polynomials was used on each dividing line. A trapezoidal formula was used for the Fourier analysis of a_{mn} and b_{mn}, and N was set as 4. Figure 5b is the equimoment diagram produced by the method. Comparing the diagram with the equimoment diagram of Fig. 5a obtained by the interpolation of the measured value of the moment, we notice that the mathematical expression represents the global characteristics of the experimentally obtained moment of force.

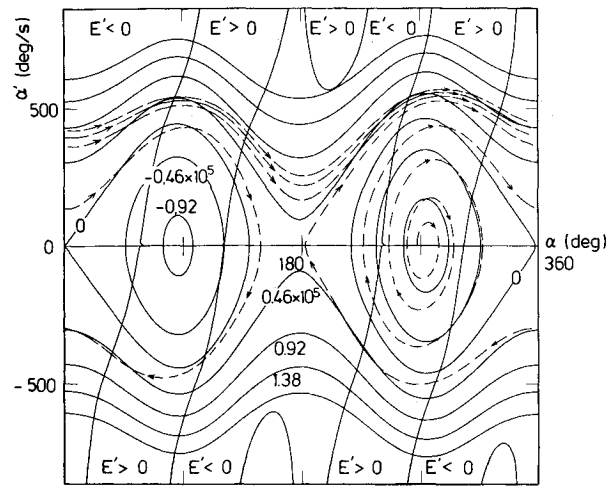

Fig. 7 Equitotal energy diagram and border lines ($E'=0$). The difference of E/I and U/I between lines $=0.46\times10^5$ (deg/s)^2. --- Trajectory calculated by the mathematical expression of moment of force.

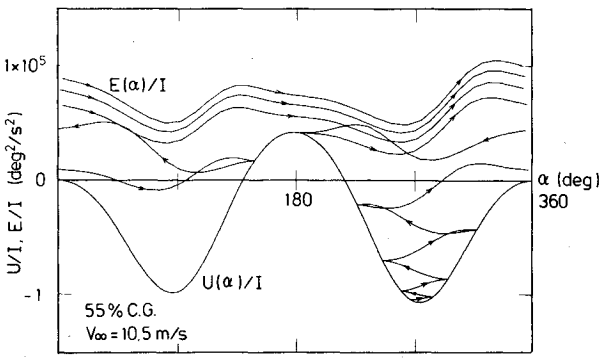

Fig. 8 Variation of potential energy and total energy of the model in angular motion.

Figure 6 shows the angular motion obtained by integrating Eq. (2), using the values of a_{mn} and b_{mn}. It reproduces fairly well the pitching motion observed in the experiment in Fig. 2a.

Lines of constant energy based on Eqs. (3) and (4) on the phase plane are shown in Fig. 7. Energy is at a minimum at equilibrium angles near 90 and 270 deg. The border lines of the energy-increasing zone ($E'>0$) and energy-decreasing zone ($E'<0$) are drawn in Fig. 7. In this figure, the calculated trajectory of the angular motion is also shown. Crossing the equienergy curves outward in the energy increasing region and crossing them inward in the energy decreasing region, the motion transfers from an oscillation to a rotation.

In Fig. 8, the potential energy for the model given by Eq. (4) as a function of α is shown as well as the change of the total energy in angular motion. The motion of the body changes from oscillation to steady rotation, repeating the increase and decrease of its total energy after starting from the equilibrium point where the potential energy is at a minimum. Even in the steady rotation, the total energy of the model varies periodically since there is transfer of energy between the model and the flow.

It is important to note that the expression of the moment derived here as $m_A = I\alpha'' = f(\alpha, \alpha')$ for the pitching motion of a body is valid only for that particular value of the moment of inertia I. It will be generalized by experiments for models with the same shape but different I.

Flow Visualization

To find the cause of the dynamically unstable pitching motion, the flowfield over the leeward side of the model was visualized by titanium tetrachloride. Figure 9 shows a series of photographs taken from 16 mm moving pictures of one cycle of a pitching oscillation. In Fig. 9a, the reattached vortices are observed along the leeward side at an angle of attack of 45 deg. As the angle of attack increased, the asymmetric separation of vortices also increased. Three distinct regions are observed in Fig. 9b at the angle of attack of 62 deg: a vortex separated on the nose-cone section, a vortex separated on the cylindrical section, and a flow about the base section. In Fig. 9c the flow is about to separate at the tip of the nose

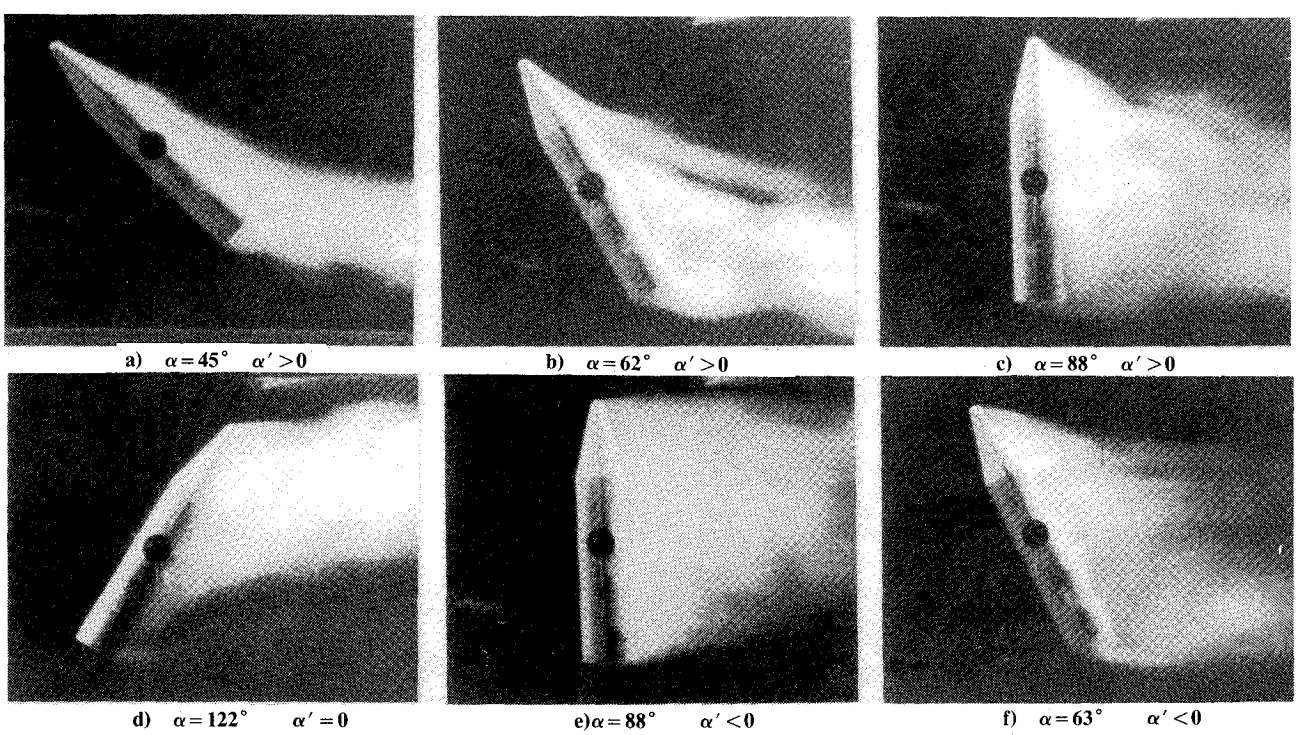

Fig. 9 Flow visualization of leeward side of the standard cone- cylinder model by titanium tetrachloride in a cycle of pitching motion about 55% c.g. at $V_\infty = 8.2$ m/s.

along the freestream direction at the angle of 88 deg. Near the angle of attack of 90 deg the streamline which separates at the forward corner of the base begins to approach the leeward corner of the base. The axial velocity component along the leeward side of the model changes its direction, heading from the base to the nose. After taking the base-first attitude at the maximum angle of attack as shown in Fig. 9d, the model decreases the angle. In Fig. 9e, cross flow covers the model and the base flow still attaches to the base surface, in contrast to Fig. 9c. There is a difference of about 10 deg between the angles when the base flow separated and when it reattached. The separated flows on the lee side of the nose do not reattach to the nose until the angle of attack decreases to 63 deg as shown in Fig. 9f, causing a stall and a decrease of the moment of force. The difference between the angles is about 25 deg. These facts suggest that the delay in separation and reattachment of the flow behind the model in a dynamic cycle of the pitching motion is one of the causes of the diverging motion.

Angular Motion of Several Axisymmetric Bodies

Cone-Cylinder Models (25 mm Diameter)

The effect of the position of the center of gravity was tested. When the center of gravity of the standard cone-cylinder model ($\theta/2 = 15$ deg, $D = 25$ mm, $l = 135$ mm) was transferred to a point 60% from the nose, the pitching motion drew trajectories as shown in Fig. 10. One of the equilibrium angles of attack is slightly greater than 90 deg and the other is slightly less than 270 deg; a base-first attitude is equilibrium. The amplitude of the angular oscillations about the equilibrium angles of attack slowly increased through several oscillations, in contrast to the model set at 55% c.g. Then an oscillation with greater amplitude began about the angle of attack of 180 deg. After almost four oscillations the model began to rotate in one direction, finally approaching a steady rotation.

In Fig. 11, the variation of the moment as functions of α for 55 and 60% c.g. is shown, where $\alpha' = 0$ and $V_\infty = 10.5$ m/s. For 55% c.g., the absolute value of the maximum pitching moment in the region of the base-first angle ($90 < \alpha < 180$ deg) is greater than the absolute value of the maximum of that in the region of the nose-first angle ($0 < \alpha < 90$ deg). For 60% c.g., the situation is reversed. When the center of gravity moved much further to the nose side or to the base side, the model did not rotate but oscillated about the angle $\alpha = 0$ or 180 deg.

Figure 12 shows the variation of the pitching moment coefficient as a function of the angle of attack at different freestream velocities for a standard cone-cylinder model at the center of gravity of 55% and at $\alpha' = 0$. The difference of the moment coefficient due to freestream velocity is small in the low-speed flow.

Figure 13 shows the variation of the pitching moment coefficient as a function of α for models with the nose angle $\theta/2 = 10$, 15, and 20 deg at $\alpha' = 0$ whose centers of gravity are at 55% from the nose tips. As the nose angle of the model decreases the pitching moment coefficients between $\alpha = 0$ and 90 deg decrease remarkably, since the center of pressure moves to the base side. On the other hand, the moment coefficients at α between 90 and 180 deg remain almost the same. The results show that the forward shapes of the model in the flow have predominant effect on the coefficient.

Bicone Models (25 mm Diameter)

To study the contribution of the nosecone of cone-cylinder models to the pitching motion, models with the same nosecone heads of $\theta/2 = 10$ and 20 deg on both ends were tested by supporting them at the center (50% c.g.). After the oscillation, all of these models rotated easily about the equilibrium angle of attack of 90 and 270 deg. The dotted line in Fig. 14 indicates the measured trajectory of an angular

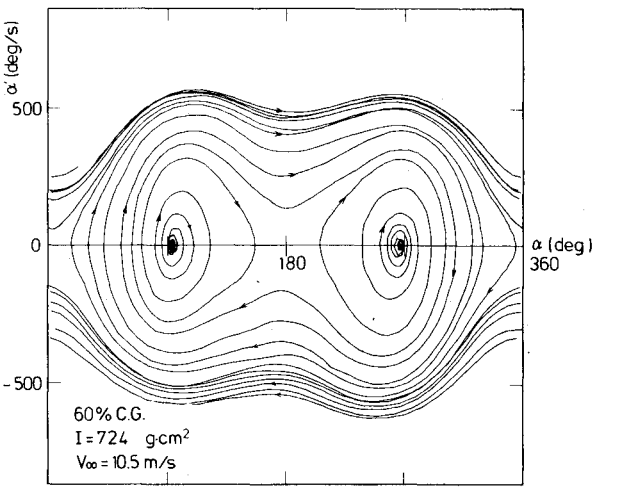

Fig. 10 Trajectories of two angular motions about 60% c.g. of the standard cone-cylinder model at $V_\infty = 10.5$ m/s.

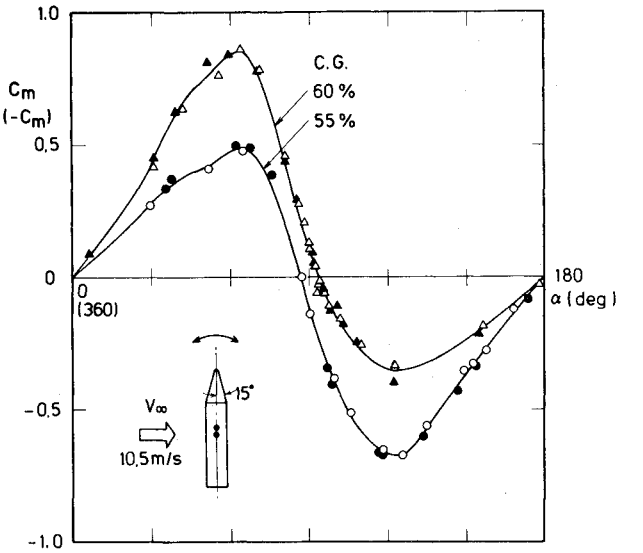

Fig. 11 Variation of pitching moment coefficient of the standard cone-cylinder model at $\alpha' = 0$ for different centers of gravity. For 55% c.g., $I = 586$ g.cm^2 and for 60% c.g., $I = 724$ g.cm^2.

motion of the bicone model with the nose angle $\theta/2 = 10$ deg on a phase plane where, after the oscillation, the model changes to rotation about the equilibrium angle of 90 deg. The oscillation about the angle of 0 and 180 deg was not observed with bicone models. Since the model is symmetric about the center of gravity, it is to be expected that the aerodynamic characteristics are symmetric about $\alpha = 0$, 90, 180, and 270 deg.

Figure 14 is an analytically expressed equienergy diagram showing the symmetry of the aerodynamic characteristics. The small irregularity of the model and the coating on the surface are thought to be the cause of the slight asymmetry. The difference in potential at $\alpha = 0$ and 360 deg shows that the model rotates easily in one direction. The phase plane is divided into energy-increasing regions ($E' > 0$) and energy-decreasing regions ($E' < 0$), where the energy is transferred alternately between the model and the flow. The measured trajectory of the angular motion on the phase plane crosses the equienergy curves outward in the region of increasing energy and inward in the decreasing region. This fact shows that the analytically expressed physical characteristics obtained from the measured data can express the features of the angular motions well.

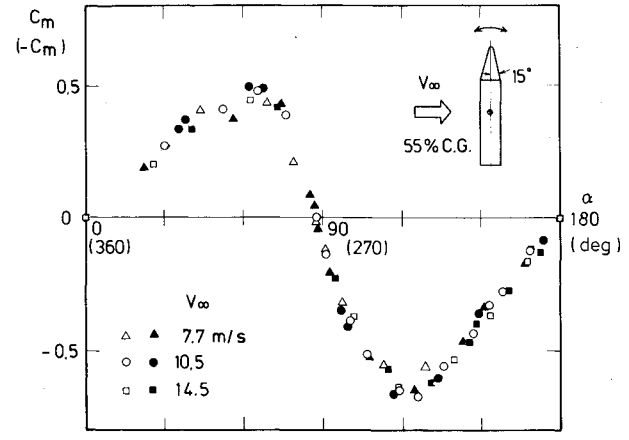

Fig. 12 Variation of pitching moment coefficient at $\alpha' = 0$ for different freestream velocity.

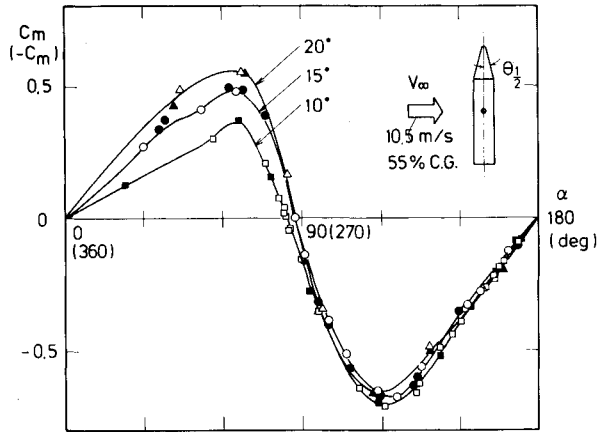

Fig. 13 Variation of pitching moment coefficient at $\alpha' = 0$ for different half nose angles; $\theta 1/2 = 10$, 15, and 20 deg.

Figure 15 shows the moment coefficient of the bicone models with $\theta 1/2 = 10$ and 20 deg as the functions of α at $\alpha' = 0$ and $V_\infty = 10.5$ m/s. In Figs. 14 and 15, the symmetry about $\alpha = 90$ deg is almost preserved. The ratio of the maximum pitching moment coefficients for $\theta 1/2 = 20$ and 10 deg is about 1.35; which is greater than the ratio of the planform areas, 1.24.

Flat-Face Cylinder Models and Hemispherical Cylinder Model

To study the effect of the flat-face nose section of the slender model, cylinder models with diameters of 10, 15, 20, and 25 mm and length $l = 130$ mm were tested by supporting them at the centers. As was pointed out by Bustemante and Stone,[11] the cylinders can hardly rotate. Most of the models stayed in an angular oscillation about $\alpha = 90$ and 270 deg, even though they were rapidly accelerated away from the angle. The model with a diameter of 20 mm only rotated. The flat face of the nose seems to suppress the pitching rotation.

The model with the hemispherical shapes on both ends of a cylinder also rotates as a bicone cylinder model. The steady rotation rate of the model was similar to that of the bicone cylinder model with a nose angle of $\theta 1/2 = 10$ deg.

Large Cone-Cylinder Model (50 mm Diameter)

To reduce the effect of blockage, a bigger cone-cylinder model ($\theta 1/2 = 15$ deg, $l = 275$ mm, $D = 50$ mm) was tested in a larger wind tunnel. To prevent vibration, eight wires were used to support the model. The experiment shows that there is

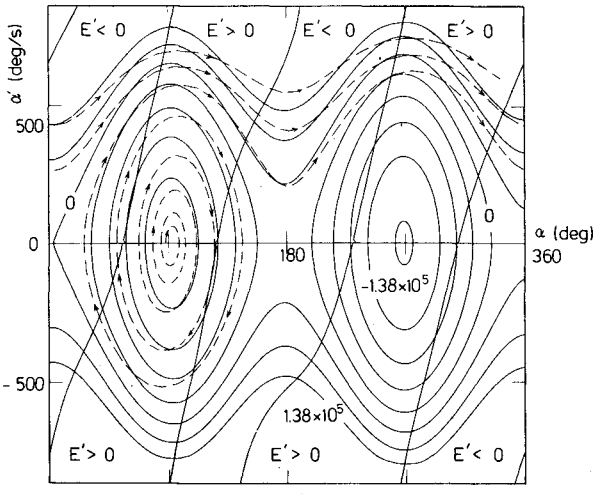

Fig. 14 Equienergy diagram with border lines ($E' = 0$) and a measured trajectory of pitching motion of bicone cylinder model with $\theta 1/2 = 10$ deg. Difference of U/I and E/I between the lines $= 0.46 \times 10^5$ (deg/s)^2.

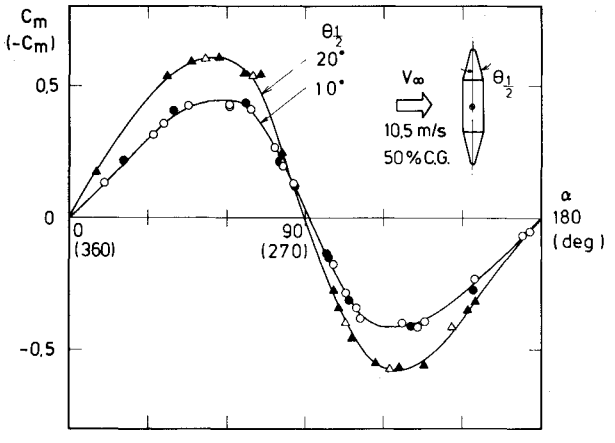

Fig. 15 Moment coefficient of bicone cylinder models with $\theta 1/2 = 10$ and 20 deg at $\alpha' = 0$ and $V_\infty = 10.5$ m/s. For $\theta 1/2 = 10$ deg, $I = 271$ g.cm^2 and for $\theta 1/2 = 20$ deg, $I = 483$ g.cm^2.

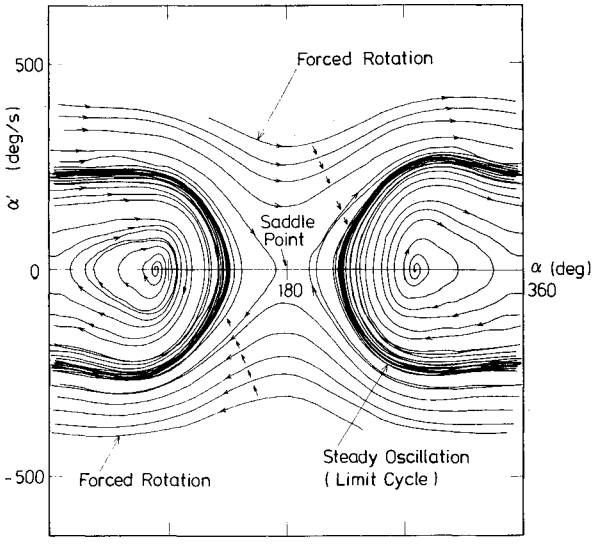

Fig. 16 Trajectories of pitching motion of greater cone-cylinder model ($\theta 1/2 = 15$ deg, $l = 275$ mm, $D = 50$ mm) around 50% c.g. at $V_\infty = 20$ m/s. $I = 3.00 \times 10^4$ g.cm^2.

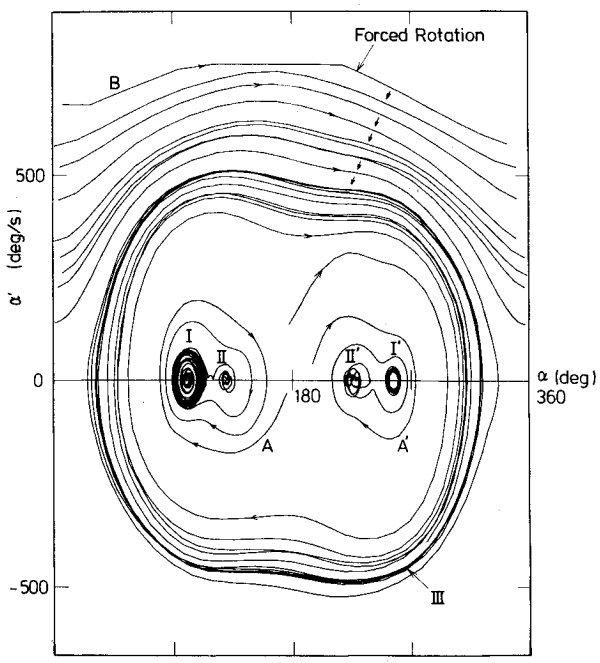

Fig. 17 Trajectories of pitching motion of greater cone-cylinder model around 62.7% c.g. at $V_\infty = 19.8$ m/s. $I = 2.23 \times 10^4$ g.cm^2.

an upper limit to the Reynolds number under which the cone-cylinder model can continue steady rotation. For this model, with the centers of gravity between 55 and 60% from the nose tip, the maximum Reynolds number is about 10^5. Most of the pitching motions, including rotation, are similar to those for the smaller model. Two examples of somewhat different angular motions are shown.

Figure 16 shows four trajectories of the pitching motion with the 50% c.g. at a freestream velocity of 20 m/s. The model initially oscillated around the equilibrium angles $\alpha_{e1} = 80.5$ deg and $\alpha_{e2} = 279$ deg then began larger oscillations about the angle of 0 deg but did not rotate. In the region where the trajectories approach each other, there is a limit cycle of the first kind. Two trajectories initially forced to rotate but finally changed to oscillations are also shown. Although not shown here, the trajectories calculated by the analytic expression of the moment of force based on the experimental data also give almost the same trajectories.

Figure 17 shows six trajectories with the center of gravity at 62.7% and $V_\infty = 19.8$ m/s. In this case the angular motion is rather complicated. Since the center of gravity moves in the basewise direction compared with 50% c.g., equilibrium angles α_e exist in the range $90 < \alpha < 270$ deg, i.e., a base-first attitude. It is interesting to note that there are two kinds of equilibrium angles or limit cycles I and II. Also, near the symmetric points with respect to 180 deg, there exist other similar regions I′ and II′. Near the angles $\alpha_{e1} = 101$ deg and $\alpha_{e2} = 257$ deg, defined as the first equilibrium angles, the model showed angular oscillations converging to limit cycles I or I′. Sometimes, the model changed from one range (I or I′) to another range (II or II′) including the angle of attack near 129 or 226 deg defined as the second equilibrium angles, where the model showed irregular oscillations and sometimes returned to region I or I′. Even when the model was oscillating with greater amplitude about the region, the oscillation converged to the region as shown in the figure (A and A′). The oscillation with much greater amplitude approach a greater limit cycle III about 180 deg ranging from 32 to 324 deg. Between the regions there might be some border which divides the angular motion into greater or smaller limit cycle. A trajectory approaching the limit cycle of oscillation after the forced rotation is also shown as B in Fig. 17.

Concluding Remarks

A method to determine the pitching moment coefficient of slender bodies with less support effect was developed by simulating the pitching motion in wind tunnels as a 1-DOF angular motion. The pitching moment acting on a body was regarded as a one-valued function of an angle of attack α and its time derivative α'. The concept of a phase plane proved to be useful for the analysis of the pitching motion. The pitching moment was expressed in mathematical terms, which enabled the pitching motion to be calculated by integrating the equation of motion with an arbitrary initial condition. The present method might be useful not only in the study of pitching motion of axisymmetric bodies but also in studying the autorotation of wings.

References

[1] Ericsson, L.E. and Reding, J.P., "Steady and Unsteady Vortex-Induced Asymmetric Loads on Slender Vehicles," *Journal of Spacecraft and Rockets*, Vol. 18, March-April 1981, pp. 97-109.

[2] Reding, J.P. and Ericsson, L.E., "Maximum Side Forces and Associated Yawing Moments on Slender Bodies," *Journal of Spacecraft and Rockets*, Vol. 17, Nov.-Dec. 1980, pp. 515-521.

[3] Marcolm, G.N. and Clarkson, M.H., "Wind Tunnel Testing with a Rotary-Balanced Apparatus to Simulate Aircraft Spin Motions," *Proceedings of AIAA 9th Aerodynamic Testing Conference*, Arlington, Tex., June 1976, pp. 143-156.

[4] Kubota, H., private communication, Nov. 1978.

[5] "Investigation on High-Angle-of-Attack Aerodynamic Characteristics of a Payload of a Sounding Rocket for Material Processing Experiments. III, On a Flat-Spin in an Airdrop Test," Research Group for Recovery of Sounding Rocket Payloads, NAL TM-426, Dec. 1980 (in Japanese).

[6] Yoshinaga, T., Tate, A., and Inoue, K., "Approximate Calculation of Aerodynamic Coefficients for Rotating Slender Bodies at 90 Deg Incidence," *Journal of Spacecraft and Rockets*, Vol. 19, Jan.-Feb. 1982, pp. 84-86.

[7] Kubota, H., Arai, I., and Matsuzaka, M., "Flat Spin of Slender Bodies at High Angles of Attack," *Journal of Spacecraft and Rockets*, Vol. 20, March-April 1983, pp. 108-114.

[8] Yoshinaga, T., Tate, A., and Inoue, K., "Coning Motion of Slender Bodies at High Angles of Attack in Low Speed Flow," AIAA Paper 81-1899, Albuquerque, N. Mex., Aug. 1981.

[9] Smith, A.M.O., "On the Motion of a Tumbling Body," *Journal of Aeronautical Science*, Vol. 29, Feb. 1953, pp. 73-84.

[10] Smith, L.H. and Nunn, R.H., "Aerodynamic Characteristics of an Axisymmetric Body Undergoing a Uniform Pitching Motion," *Journal of Spacecraft and Rockets*, Vol. 13, Jan. 1976, pp. 8-14.

[11] Bustemante, A.C. and Stone, G.W., "The Autorotation Characteristics of Various Shapes for Subsonic and Hypersonic Flows," AIAA Paper 69-132, New York, Jan. 1969.

[12] Ramachandra, S.M., Sudhakar, K., and Kiran, N.S., "Lift and Pitching Moment Characteristics of Stores Determined from Flight Drop Tests," *Journal of Aircraft*, Vol. 17, Sept. 1980, pp. 663-667.

[13] Smith, E.H., "Autorotating Wings: an Experimental Investigation," *Journal of Fluid Mechanics*, Vol. 50, Part 3, 1971, pp. 513-534.

[14] Iversen, J.D., "Autorotating Flat-Plate Wings: The Effect of the Moment of Inertia, Geometry and Reynolds Number," *Journal of Fluid Mechanics*, Vol. 92, Part 2, 1979, pp. 327-348.